catalysts

MDPI

Article

Characterization and Comparative Performance of TiO_2 Photocatalysts on 6-Mercaptopurine Degradation by Solar Heterogeneous Photocatalysis

Luis A. González-Burciaga [1], Cynthia M. Núñez-Núñez [2], Miriam M. Morones-Esquivel [3], Manuel Avila-Santos [4], Adela Lemus-Santana [4] and José B. Proal-Nájera [1,*]

1 Instituto Politécnico Nacional, CIIDIR-Unidad Durango, Calle Sigma 119, Fracc. 20 de Noviembre II, Durango 34220, Mexico; luis.gonzalez.iq@gmail.com
2 Universidad Politécnica de Durango, Carretera Durango-México km 9.5, Col. Dolores Hidalgo, Durango 34300, Mexico; cynthia_cnn@hotmail.com
3 Facultad de Ciencias Forestales, Universidad Juárez del Estado de Durango, Río Papaloapan, Col. Valle del Sur, Durango 34120, Mexico; me_mirelle@hotmail.com
4 Instituto Politécnico Nacional, CICATA-Unidad Legaria, Calzada Legaria 694, Delegación Miguel Hidalgo, Ciudad de México 11500, Mexico; m.avilawinter@gmail.com (M.A.-S.); adelale@gmail.com (A.L.-S.)
* Correspondence: jproal@ipn.mx; Tel.: +52-618-134-1781

Received: 20 December 2019; Accepted: 7 January 2020; Published: 14 January 2020

Abstract: The crystallographic properties of two titanium dioxide (TiO_2) photocatalysts, P25, and commercial C1-TiO_2 reactive grade, were analyzed by X-ray diffraction (XRD) and the band-gap was calculated with UV–Vis spectrometry with integration sphere. Then, their performance was tested in the degradation of 6-mercaptopurine (6-MP) by heterogeneous photocatalysis with solar radiation under different pH conditions and the addition of hydrogen peroxide (H_2O_2); the degradation efficiency was monitored by UV–Vis spectrophotometry. The XRD analysis showed that both photocatalysts studied have anatase phase, while only P25 contains rutile; the band gap values were lower, in both catalysts, than those reported for catalysts obtained by the sol-gel method. With both photocatalysts, degradation experiments showed efficiency greater than 98% in experiments in the presence of H_2O_2 regardless of pH. The properties of the photocatalysts, along with the data obtained from the experimentation, helped determine the best semiconductor for the degradation of 6-MP with these operating conditions in this work.

Keywords: kinetics; radiation; anatase; rutile; band-gap; titanium dioxide

1. Introduction

Advanced oxidation processes (AOP), heterogeneous photocatalysis among them, are emerging alternative technologies developed to remove or degrade recalcitrant organic compounds present in wastewater [1,2]; such compounds have high chemical stability and/or low biodegradability. AOPs are based on the generation of strongly reactive radical species, like hydroxyl radicals (•OH, standard electrode potential varied between +1.8 and +2.8 V_{NHE}), which degrade a wide range of organic pollutants quickly and non-selectively into non-toxic products like CO_2, H_2O and inorganic compounds [1–3]. Among the recalcitrant organic pollutants, the antineoplastic agent 6-mercaptopurine (6-MP) was the target of this work.

The 6-MP is mainly used for the treatment of acute lymphoblastic leukemia [4], to extend the duration of remission achieved with other medications [5], which can last from 2 to 3 years after diagnosis [6]. The dose required for maintenance therapy in patients with remission is 75 mg/kg/day in the United Kingdom, the Nordic countries and the United States [4,6], while in most of Europe the

initial dose is 50 mg/kg/day [6]. 6-MP is also used in diseases such as intestinal arterial insufficiency, Crohn's disease, ulcerative colitis and inflammatory bowel disease with doses ranging from 1 to 2.5 mg/kg/day [7,8]. Due to their characteristics and high doses, removing chemicals as 6-MP has become a challenge.

Heterogeneous photocatalysis has attracted great attention in the last decade [9], is considered as one of the most attractive options for wastewater treatment due to its great potential and high efficiency through the use of solar radiation [10,11] to remove organic pollutants in aquatic systems [11,12]. In photocatalysis, a semiconductor is activated by a photon which causes the excitation of electrons in the valence band and their migration to the conduction band, thus generating highly energetic electron-hole pairs (e^-/h^+) [10,13–15]. The separation between the conduction band and the valence band, called "band-gap" or energy gap (Eg), is one of the most important results in semiconductor physics. In a simple way, Eg is evaluated from the graph obtained from the maximum limit of the valence band and the lowest limit of the conduction band, and strongly affects semiconductor properties.

Among a large number of photocatalysts used today, TiO_2 has been proven to be the most suitable for wide environmental and energy applications because of its appropriate valence band and conduction band positions, its low cost, non-toxic nature, strong oxidizing power, it is chemically inert, chemical and photo corrosion-resistant and, especially, its ability to use natural and renewable solar UV energy; therefore, it is the semiconductor with the highest application in heterogeneous photocatalysis [9,10,15–18]. However, TiO_2, as photocatalyst, presents a great disadvantage: in the absence of electron acceptors, the recombination of the electron and the hole occurs. To avoid such recombination, the addition of chemical oxidants has been used in the past; H_2O_2, for example, can react with electrons in the conduction band and prevent such recombination [15].

TiO_2 has three crystalline phases: rutile (tetragonal), anatase (tetragonal) and brokite (orthorhombic). Rutile is the only thermodynamically stable phase, while anatase and brokite are metastable. However, anatase generally shows a higher photocatalytic activity even though it has a lower ability to absorb light, due to its larger band-gap (3.2 eV) compared to rutile (3.0 eV) [17–21]. Such an effect could be due to rutile's larger grain size, lower specific surface and lower surface absorption capacity [18].

The applications of TiO_2 and its photocatalytic activity are determined by its properties, in particular, its crystallite size, specific surface area, defects and porous structure [17,18]. The particle size and characteristics data can be obtained by means of the XRD technique since they are related to the amplitude of the diffraction peaks, which in turn allows the crystalline phase identification [20]. The crystallite properties, as well as the magnitude of band-gap have been reported as examples of an intensive characterization of TiO_2 [21].

The objective of this work was to characterize two TiO_2 photocatalysts, P25, and commercial C1-TiO_2, by means of XRD and their band-gap. Afterwards, their performances on 6-MP degradation by solar heterogeneous photocatalysis were compared through kinetic analysis, based on its crystallographic properties, its magnitude of band-gap, different pH quantities and the addition of H_2O_2.

2. Results

2.1. Structural Analysis of Photocatalysts

Figures 1 and 2 show the XRD patterns for P25 and C1-TiO_2 catalysts. The red dots show the experimental data, the black line corresponds to the pattern calculated according to the method of Le Bail et al. [22], and in blue the difference between the two patterns. The vertical bars in green correspond to the Bragg positions of the anatase phase (JCPDS file 00-021-1272 of the ICDD database), which is present in both photocatalysts. In the case of TiO_2 P25, in addition to anatase, the rutile phase was found (JCPDS file 01-070-7347 of the ICDD database); it is represented by vertical red bars.

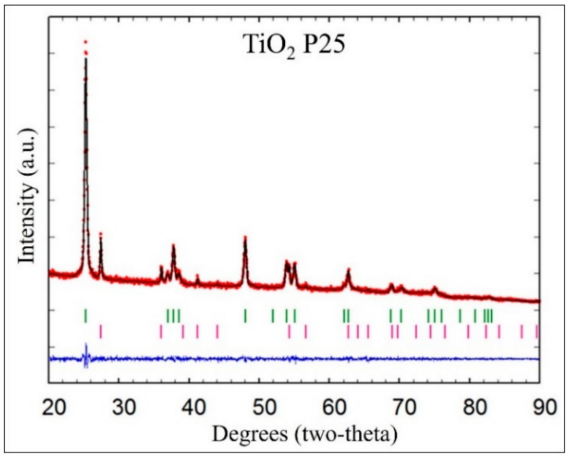

Figure 1. X-ray diffraction (XRD) pattern for TiO_2 P25. The green vertical bars correspond to the TiO_2 anatase phase, JCPDS 00-021-1272; while the red vertical bars correspond to TiO_2 rutile, JCPDS 01-070-7347.

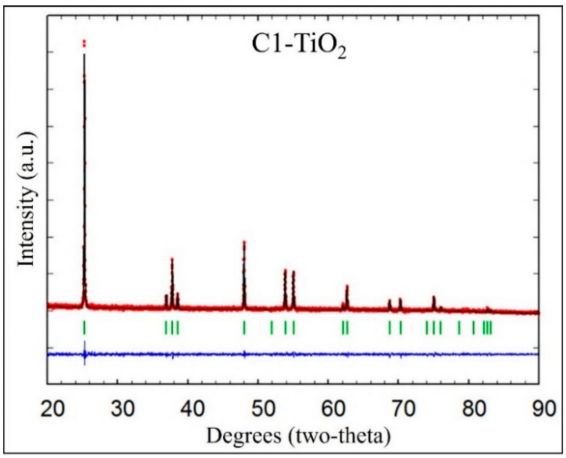

Figure 2. XRD pattern for the commercial C1-TiO_2 sample. The green vertical bars correspond to the TiO_2 anatase JCPDS 00-021-1272 phase.

One of the most robust tools for the treatment of the width of the diffraction maxima is the approximation of integral amplitude applied to the Warren–Averbach method [23]. Through this method and its implementation in the FullProf software (April-2018 version, Laboratoire Léon Brillouin CEA-CNRS, Gif-sur-Yvette, France), it was possible to calculate the crystallographic properties for both photocatalysts: the crystallite size, its average shape, the percentage of each phase and the tensions caused by structural defects, shown in Table 1.

Table 1. Crystallographic properties of TiO_2 P25 and C1-TiO_2 through XRD.

Photocatalyst	Crystalline Phase	Space Group	Phases Percentage	Crystalline Size (nm)	Crystalline Form
TiO_2 P25	Tetragonal (anatase)	I 4_1/a m d [141]	85.27	20.97	Spherical
	Tetragonal (rutile)	$P4_2$/m n m [136]	14.73	33.96	Spherical
C1-TiO_2	Tetragonal (anatase)	I 4_1/a m d [141]	100	80.71	Spherical

The absorbance spectra obtained from the photocatalysts via UV-Vis spectrophotometry with integration sphere, were treated by the modified Kubelka–Munk method, obtaining the graphic representation $[F(R)\hbar\upsilon]^2$ against $\hbar\upsilon$ where, when projecting the linear part of the curve to the energy axis, allowed the determination of the magnitude of the band opening of semiconductor energy or

band-gap needed to produce the energy gap that promotes the formation of the ·OH radicals necessary for photocatalysis [24].

Figures 3 and 4 show the graphs composed of the absorbance spectrum and the band-gap calculation for C1-TiO_2 and TiO_2 P25 made with Origin Pro 8 software (OriginLab, Northampton, MA, USA), these being lower than the values shown in the semiconductors obtained by the sol-gel method with titanium tetrabutoxide (TBT) and titanium tetraisopropoxide (TIPT) as precursors, which have values of 3.40 eV and 3.38 eV respectively [14,25]. These results indicate a faster activation of the photocatalysts TiO_2 P25 and C1-TiO_2 to the exposure to high radiation emission, in this case, solar energy.

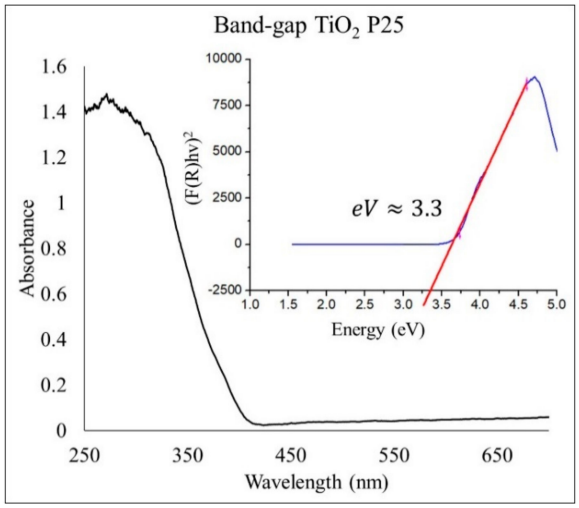

Figure 3. Band-gap calculation, according to the absorbance spectrum of TiO_2 P25, by means of the graphic representation $[F(R)\hbar\upsilon]^2$ against $\hbar\upsilon$ of the Kubelka–Munk method.

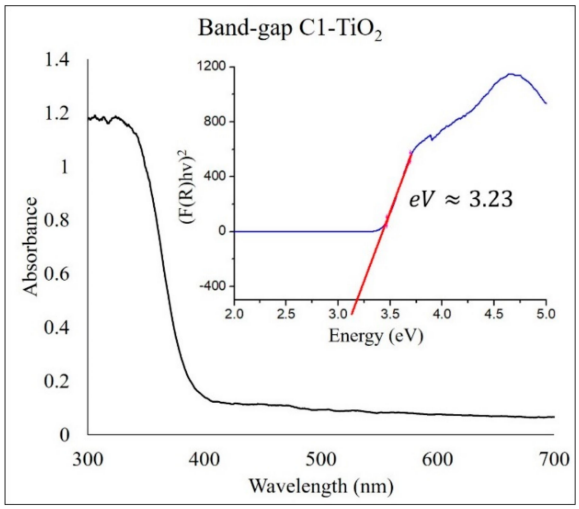

Figure 4. Band-gap calculation, according to the absorbance spectrum of C1-TiO_2, by means of the graphic representation $[F(R)\hbar\upsilon]^2$ against $\hbar\upsilon$ of the Kubelka–Munk method.

2.2. Comparison of Semiconductors Performance in 6-MP Degradation

Figure 5 shows the comparison of degradations in experiments carried out in the 1/10 m^2 reactor (reactor 1) with the photocatalysts C1-TiO_2 and TiO_2 P25 at two different pH (3.5 and 7), with a dose of 3 mM H_2O_2 in all cases. The processes performed in the absence of H_2O_2 did not show degradation of 6-MP. It also shows the control carried out without radiation to rule out that H_2O_2 has some effect on its own. With respect to the basic pH 9.5, the initial concentrations could not be reached because 6-MP is an acidic drug with a pKa of 7.7 [26,27], therefore, when applying the

Henderson–Hasselbalch equation [28–30], an ionization of the compound of 98.4% was obtained after adjusting the pH, indicating that the molecule dissociates at high pH. When analyzing the experimental runs with a pH 3.5, a better degradation was found and, in addition, the steeper concentration drop occurs much faster; as can be seen in the graph, it happens around five minutes after the start of the experiment.

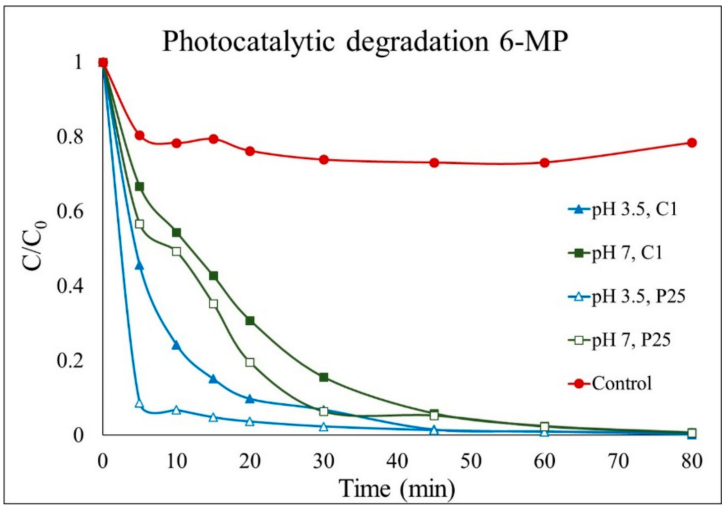

Figure 5. Degradation of 6-mercaptopurine (6-MP) after 80 min of reaction in a flat-bed reactor with an area of 1/10 m^2, with two photocatalysts (TiO_2 P25 and C1-TiO_2), two pH magnitudes (3.5 and 7) and a H_2O_2 dose of 3 mM.

The high degradation efficiencies of 6-MP are mainly due to the characteristics of the photocatalysts, its particle size in the order of nanometers and their spherical shape without defects or structural tensions are essential for optimal photocatalytic activity [31]. Next to this, the high radiation in the city of Durango plays an important role in the activation of the semiconductor, considering that the average intensity during the experiments was 878 W/m^2.

Once it was determined that pH 3.5 and a H_2O_2 dose of 3 mM yielded better 6-MP degradation results that other conditions tested, experiments were carried out in the 1 m^2 reactor (reactor 2) with the two photocatalysts. The data show that there is no difference in drug degradation between the use of TiO_2 P25 and C1-TiO_2, as the final degradation is similar to that obtained in the smaller surface reactor. However, greater contaminant removal was reached in reactor 2 before 20 min of having started the experiment, with an average radiation of 662 W/m^2; while with reactor 1, the greatest degradation was obtained between 45 and 55 min.

Table 2 concentrates the degradation efficiencies of 6-MP in solar heterogeneous photocatalysis experiments. As can be seen by comparing only the final performance of the experiments with TiO_2 P25 and C1-TiO_2 in the same reactor with the same operating conditions, there is no remarkable difference between these when analyzing the 6-MP removal rates. However, when observing the experimentation times between 5 and 50 min in Figure 5, it can be noted that there was a more pronounced drop in contaminant concentration with P25 compared to C1.

Regarding COD, the highest removal (67%) was reached by experiment in reactor 1, under initial pH 7 and with P25 as photocatalyst. The other experiments in reactor 1 showed lower COD removal (5%–45%). In reactor 2, similar results were observed.

On the other hand, when analyzing the degradation kinetics, a difference can be observed in the photocatalytic operational constants and the half-life in the reactor 1, demonstrating that TiO_2 P25 had a better performance than C1-TiO_2 at both pH with a H_2O_2 dose of 3 mM. In the case of reactor 2, with a pH 3.5 and the same dose of H_2O_2, the kinetic data show a difference between photocatalysts much smaller than that observed in reactor 1 (Table 3).

Table 2. Degradation efficiencies of 6-MP in aqueous solution by solar heterogeneous photocatalysis with two photocatalysts: TiO_2 P25 and C1-TiO_2. 6-MP initial concentration was 25 mg/L in all experiments.

Reactor	[1] Phc	[2] Exp. (H_2O_2 3 mM)	[3] $\hbar\upsilon$ (W/m^2)	λ = 324 nm [4] (%Deg)
1/10 m^2	P25	pH 3.5	904.85	99.27
		pH 7.0	909.84	99.38
	C1	pH 3.5	925.67	99.79
		pH 7.0	865.80	99.27
1 m^2	P25	pH 3.5	773.32	99.09
	C1	pH 3.5	551.60	98.55

[1] photocatalyst, [2] experimental parameters, [3] solar radiation, [4] degradation percentage.

Table 3. Data on the degradation kinetics of 6-MP by solar heterogeneous photocatalysis with two TiO_2 photocatalysts in two reactors with different surfaces *.

Reactor	[1] Phc	pH	[2] K_{op} (min^{-1})	[3] τ (min)
1/10 m^2	P25	3.5	0.2812	2.4652
		7.0	0.0838	8.2747
	C1	3.5	0.1351	5.1321
		7.0	0.0643	10.7785
1 m^2	P25	3.5	0.3361	2.0623
	C1	3.5	0.3158	2.1949

* Only experiments with a H_2O_2 dose of 3 mM are shown. [1] photocatalyst, [2] operational photocatalytic constant, [3] half-life time.

Considering the characteristics of the photocatalysts and the parameters of the experiments, C1-TiO_2 would be expected to have a superior performance in the degradation of 6-MP compared to TiO_2 P25, this because it has only the anatase phase in its composition, which usually exhibits the highest photocatalytic activity compared to rutile under equal conditions [18,32,33]. However, several authors demonstrate that other parameters can affect how semiconductors behave and their photocatalytic activity varies due to these.

Some studies have indicated that anatase concentration is not very important when you have a very small particle size [34]; on the other hand, depending on the nature and characteristics of the contaminant, it is preferable, on rare occasions, to have a larger crystallite size [35,36]. It has even been confirmed that, with some substances, the photocatalytic activity of TiO_2 rutile is higher compared to that of TiO_2 anatase [37].

3. Materials and Methods

3.1. Chemical Reagents

Hydrated 6-MP reagent (Figure 6) was purchased from Cayman Chemical (Cayman Chemical, Ann Arbor, MI, USA, CAS: 6112-76-1). Photocatalysts used were TiO_2 P25, obtained from Evonik Industries (Evonik Industries AG, Essen, NRW, Germany, CAS: 13463-67-7), and commercial C1-TiO_2, obtained from a national distributor (Productos Químicos Monterrey, S.A. de C.V. FERMONT, Monterrey, N.L., Mexico, CAS: 13463-67-6). The pH adjustment of the 6-MP solutions was performed with 65% nitric acid and with sodium hydroxide at a concentration of 0.1 M, both reagents distributed by Merck (Merck, Naucalpan de Juárez, Edomex, Mexico). Purified 30% Fermont brand H_2O_2 (Productos Químicos Monterrey, S.A. de C.V. FERMONT, Monterrey, N.L., Mexico, CAS: 7722-84-1) was used as an oxidizing agent. All solutions were made with distilled water of the Hycel brand (Hycel, Zapopan, Jal., Mexico, CAS: 7732-18-5).

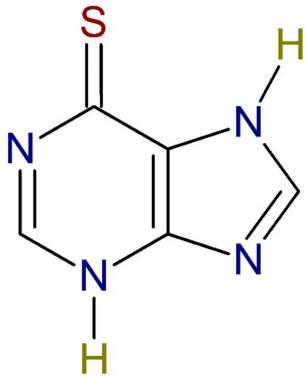

Figure 6. The 6-MP chemical structure.

3.2. TiO_2 Photocatalysts Characterization

Crystallographic analysis was carried out by XRD. The diffraction pattern was obtained in a Bruker D8 advance equipment (Bruker Corporation, Billerica, MA, USA), using a Cu-kα_1 wavelength of 1.5406 Å. The measurement was made with a range of 2θ in the angular range of 20° to 90°, with a step of 0.0289° for TiO_2 P25 and 0.0144° for C1-TiO_2 with a time per point of two seconds. The Bragg–Brentano geometry was used with a Ge (111) Johansson monochromator in the primary beam and a LynxEye detector in the secondary beam. Finally, the average crystallite size was determined from the diffraction pattern for the two photocatalysts.

Identification of the crystalline phases present in the XRD patterns was carried out by consulting the PDF-2 2016 database of the International Center for Diffraction Data (ICDD).

Calculation of the band-gap was carried out by determining the absorbance spectrum of the semiconductors at room temperature by means of a UV-visible spectrophotometer with LAMBDA 950 UV/Vis/NIR integration sphere of the Perkin Elmer brand (Perkin Elmer Inc., Waltham, MA, USA). Then, the Kubelka–Munk function was used [21], which allows converting diffuse reflectance measurements into equivalent absorbance spectra, using alumina as a reference [24].

3.3. Comparison of Semiconductor Performance in 6-MP Degradation

3.3.1. Photocatalytic Reactors

Two solar reactors with contact areas of 1/10 m^2 (reactor 1) and 1 m^2 (reactor 2) were used. Such reactors, shown in Figure 7, are formed by a metal base that supports the rest of the system with an inclination of 20°, which is close to the latitude of Durango City, Mexico (24°01′37″ N), so that the solar radiation uptake is maximized [14]. On the base, an acrylic container is supported within which frosted glass plates are placed.

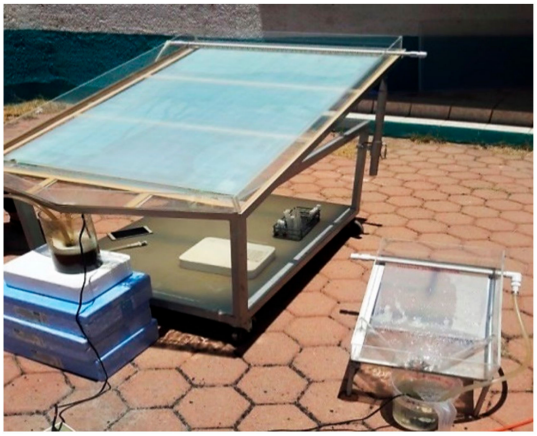

Figure 7. Solar reactors with 1 m^2 (left) and 1/10 m^2 contact surface (right).

The aqueous solution of the contaminant (6-MP) flows over the glass plates after leaving a polyvinyl chloride pipe with holes evenly separated every 5 mm. After passing through the glass, the solution falls into a glass container where it is recirculated to the reactor. Each system has a submersible pump responsible for recirculating the liquid at a constant flow, for the reactor 1, a Biopro H-330 pump is responsible for maintaining the flow at 100 L/h, while the reactor with larger surface keeps its flow at 355 L/h with a Biopro H-450 device.

3.3.2. Experimentation

The experiments were performed with samples at an initial concentration of 25 mg/L prepared with the 6-MP standard diluted in distilled water by stirring for half an hour on a magnetic stirrer. For each experiment, volumes of 2 L were prepared for reactor 1 and 3 L for reactor 2.

The frosted glass of the reactors was impregnated with the selected photocatalyst for the experiment (TiO_2 P25 or C1-TiO_2), spreading 2 g/m^2 on the glass according to the direct spray technique of Stintzing [38].

To test the effect of pH on the degradation of the contaminant, experiments were carried out at the initial pH 3.5 and 7; once the 6-MP solution was prepared, the pH was adjusted with 65% HNO_3 or 0.1 M NaOH. The pH measurements were made using an Orion Star A211 Thermo Scientific potentiometer (Thermo Fisher Scientific Inc., Waltham, MA, USA).

In addition to pH magnitude, the effect of H_2O_2 as an electron donor to avoid recombination of the electron-hole in the semiconductor surface was studied. For this purpose, experiments were carried either in absence of H_2O_2 or adding a dose of 3 mM to the solution at the beginning of each experiment. The experiments were performed by recirculating the sample on the reactor for 80 min, taking samples at times 0, 5, 10, 15, 20, 30, 45, 60 and 80 min. The 6-MP removal was followed by UV-Vis spectrophotometry in a Hach DR 5000TM (HACH Company, Loveland, CO, USA) device, at a maximum absorption of 324 nm; and for the COD degradation, the Hach 2000 method was used with a DR 2010 spectrophotometer (HACH Company, Loveland, CO, USA). In the present study, 6-MP degradation by-products were not measured as it was not part of the objectives of the work; according to consulted literature, 6-MP molecular breakdown could result in the next chemical compounds: purine-6-sulphinate, purine-6-sulphonate and hypoxanthine [39].

At the end of each experiment, the reactor was washed to remove the remains of solution; special care was taken to wash the frosted glass to remove the catalyst residues.

3.3.3. Kinetic Analysis

Kinetic analysis was performed considering a first-order reaction. The operational rate constant (K_{op}) of the photocatalytic reaction for the degradation process was determined through Equation (1) [15,40]:

$$C = C_0 e^{-K_{op} \cdot t}, \quad (1)$$

where C corresponds to 6-MP concentration at time t, C_0 represents 6-MP initial concentration of the sample and t is the time at which the sample was taken.

The kinetic curve for 6-MP degradation was obtained by a non-linear relationship (C/C_0 vs. t) for each treatment [41].

4. Conclusions

The band-gap calculation shows that the energy required for the activation of the two photocatalysts is similar; however, the XRD study determined that the particle size of TiO_2 P25 is much smaller compared to C1-TiO_2, which favors the photocatalytic activity of P25.

Rate operational constants of degradation show faster 6-MP elimination with TiO_2 P25 in the first minutes of experimentation. Comparing the two reactors, a larger surface clearly shows higher

operational constants due to a larger contact surface. It is clear that in the two reactors the best-tested parameters for the degradation of this organic compound are a pH 3.5 with a H_2O_2 dose of 3 mM.

Although this work determined the degradation of 6-MP by heterogeneous photocatalysis in a flat-bed solar photocatalytic reactor, the nature of the compounds to be degraded can modify these parameters. Therefore, it is important to determine them for each contaminant that is intended to be removed from a model or a sample of water.

Author Contributions: Data curation, L.A.G.-B.; formal analysis, L.A.G.-B., A.L.-S. and M.A.-S.; funding acquisition, J.B.P.-N.; investigation, L.A.G.-B, M.M.M.-E. and J.B.P.-N.; methodology, L.A.G.-B. and J.B.P.-N.; project administration, J.B.P.-N.; supervision, J.B.P.-N.; writing—original draft, L.A.G.-B.; writing—review and editing, C.M.N.-N. and J.B.P.-N. All authors have read and agreed to the published version of the manuscript.

Funding: The authors wish to extend their sincere appreciation to the Consejo Nacional de Ciencia y Tecnología (CONACyT) through the doctorate scholarship granted. Support was received also from Instituto Politécnico Nacional (IPN/SIP project 20190247) for funding this project. The content does not necessarily reflect the views and policies of the funding organizations.

Acknowledgments: The authors would also like to acknowledge the Planta de Tratamiento de Aguas Residuales Oriente for providing additional facilities to conduct the research, Centro de Investigación de Materiales Avanzados (CIMAV) for sample analysis and Laboratorio Nacional de Conversión y Almacenamiento de Energía (LNCAE) for access to its experimental facility.

Conflicts of Interest: The authors declare no conflict of interest.

References

1. Bokare, A.D.; Choi, W. Review of iron-free Fenton-like systems for activating H_2O_2 in advanced oxidation processes. *J. Hazard. Mater.* **2014**, *275*, 121–135. [CrossRef] [PubMed]
2. Yang, S.; Wang, P.; Yang, X.; Wei, G.; Zhang, W.; Shan, L. A novel advanced oxidation process to degrade organic pollutants in wastewater: Microwave-activated persulfate oxidation. *J. Environ. Sci.* **2009**, *21*, 1175–1180. [CrossRef]
3. Fasnabi, P.A. Studies on Advanced Oxidation Processes for the Removal of Acetamiprid from Wastewater. Ph.D. Thesis, Cochin University of Science and Technology, Kerala, India, 2015.
4. Schmiegelow, K.; Bretton-Meyer, U. 6-mercaptopurine dosage and pharmacokinetics influence the degree of bone marrow toxicity following high-dose methotrexate in children with acute lymphoblastic leukemia. *Leukemia* **2001**, *15*, 74–79. [CrossRef] [PubMed]
5. Lennard, L.; Rees, C.A.; Lilleyman, J.S.; Maddocks, J.L. Childhood leukaemia: A relationship between intracellular 6-mercaptopurine metabolites and neutropenia. *Br. J. Clin. Pharmacol.* **1983**, *16*, 359–363. [CrossRef]
6. Schmiegelow, K.; Nielsen, S.N.; Frandsen, T.L.; Nersting, J. Mercaptopurine/Methotrexate maintenance therapy of childhood acute lymphoblastic leukemia: Clinical facts and fiction. *J. Pediatr. Hematol. Oncol.* **2014**, *36*, 503–517. [CrossRef]
7. Medscape. Available online: https://reference.medscape.com/drug/purinethol-purixan-mercaptopurine-342094 (accessed on 15 November 2018).
8. Drugs.com. Available online: https://www.drugs.com/dosage/mercaptopurine.html (accessed on 16 November 2018).
9. Qin, X.; Jing, L.; Tian, G.; Qu, Y.; Feng, Y. Enhanced photocatalytic activity for degrading Rhodamine B solution of commercial Degussa P25 TiO_2 and its mechanisms. *J. Hazard. Mater.* **2009**, *172*, 1168–1174. [CrossRef]
10. Sousa, M.A.; Gonçalves, C.; Vilar, V.J.; Boaventura, R.A.; Alpendurada, M.F. Suspended TiO_2-assisted photocatalytic degradation of emerging contaminants in a municipal WWTP effluent using a solar pilot plant with CPCs. *Chem. Eng. J.* **2012**, *198*, 301–309. [CrossRef]
11. Dong, S.; Feng, J.; Fan, M.; Pi, Y.; Hu, L.; Han, X.; Menglin, L.; Sun, J.; Sun, J. Recent developments in heterogeneous photocatalytic water treatment using visible-light-responsive photocatalysts: A review. *RSC Adv.* **2015**, *5*, 14610–14630. [CrossRef]
12. Constantin, L.A.; Nitoi, I.; Cristea, I.; Oancea, P. Kinetics of 5-Fluorouracil Degradation by Heterogenous TiO_2 Photocatalysis. *Rev. Chim.* **2016**, *67*, 1447–1450.

13. Tizaoui, C.; Mezughi, K.; Bickley, R. Heterogeneous photocatalytic removal of the herbicide clopyralid and its comparison with UV/H_2O_2 and ozone oxidation techniques. *Desalination* **2011**, *273*, 197–204. [CrossRef]
14. Morones, M.M.; Pantoja, J.C.; Proal, J.B.; Cháirez, I.; Gurrola, J.N.; Ávila, M. Uso de un reactor de placa plana (TiO_2/vidrio) para la degradación de 2,5-diclorofenol por fotocatálisis solar. *Rev. Int. Contam. Ambie.* **2017**, *33*, 605–616. [CrossRef]
15. Núñez-Núñez, C.M.; Chairez-Hernández, I.; García-Roig, M.; García-Prieto, J.C.; Melgoza-Alemán, R.M.; Proal-Nájera, J.P. UV-C/H_2O_2 heterogeneous photocatalytic inactivation of coliforms in municipal wastewater in a TiO_2/SiO_2 fixed bed reactor: A kinetic and statistical approach. *React. Kinet. Mech. Catal* **2018**, *125*, 1159–1177. [CrossRef]
16. Pantoja-Espinoza, J.C.; Proal-Nájera, J.B.; García-Roig, M.; Cháirez-Hernández, I.; Osorio-Revilla, G.I. Eficiencias comparativas de inactivación de bacterias coliformes en efluentes municipales por fotólisis (UV) y por fotocatálisis (UV/TiO_2/SiO_2). Caso: Depuradora de aguas de Salamanca, España. *Rev. Mex. Ing. Quím.* **2015**, *14*, 119–135.
17. Tayade, R.J.; Surolia, P.K.; Kulkarni, R.G.; Jasra, R.V. Photocatalytic degradation of dyes and organic contaminants in water using nanocrystalline anatase and rutile TiO_2. *Sci. Technol. Adv. Mater.* **2007**, *8*, 455–462. [CrossRef]
18. Zhang, J.; Zhou, P.; Liu, J.; Yu, J. New understanding of the difference of photocatalytic activity among anatase, rutile and brookite TiO_2. *Phys. Chem. Chem. Phys.* **2014**, *16*, 20382–20386. [CrossRef] [PubMed]
19. Hu, Y.; Tsai, H.L.; Huang, C.L. Phase transformation of precipitated TiO_2 nanoparticles. *Mater. Sci. Eng. A* **2003**, *344*, 209–214. [CrossRef]
20. Thamaphat, K.; Limsuwan, P.; Ngotawornchai, B. Phase Characterization of TiO_2 Powder by XRD and TEM. *Kasetsart J. Nat. Sci.* **2008**, *42*, 357–361.
21. López, R.; Gómez, R. Band-gap energy estimation from diffuse reflectance measurements on sol–gel and commercial TiO_2: A comparative study. *J. Sol-Gel Sci. Technol.* **2012**, *61*, 1–7. [CrossRef]
22. Le Bail, A.; Duroy, H.; Fourquet, J.L. Ab-initio structure determination of $LiSbWO_6$ by X-ray powder diffraction. *Mater. Res. Bull.* **1988**, *23*, 447–452. [CrossRef]
23. Warren, B.E. *X-ray Diffraction*, 1st ed.; Dover Publications: NewYork, NY, USA; EUA: Brussels, Belgium, 1990; pp. 41–67.
24. Velasco-Arias, D. Obtención De Nanoestructuras Hechas a Base De Bismuto. Cerovalente, Bi_2O_3, Bi¬$_2Mo_3O_{12}$ y $Bi_2Mo_2O_9$. Ph.D. Thesis, Faculty of Chemistry, Universidad Nacional Autónoma de México, Mexico, Mexico, 2013.
25. Sheng, Y.; Liang, L.; Xu, Y.; Wu, D.; Sun, Y. Low temperature deposition of the high-performance anatase-titania optical films via a modified sol–gel route. *Opt. Mater.* **2008**, *30*, 1310–1315. [CrossRef]
26. Sochacka, J.; Pawelczar, B. Characterization of 6-mercaptopurine binding site on human α1-acid glycoprotein (Orosomucoid) using molecular docking. *Acta Pol. Pharm.* **2012**, *69*, 161–166. [PubMed]
27. Lin, A.P.; Peng, J.D.; Zhou, M.; Zhang, J. Resonance light scattering determination of 6-mercaptopurine coupled with HPLC technique. Spectrochim. *Acta A Mol. Biomol. Spectrosc.* **2016**, *154*, 1–7. [CrossRef]
28. Horn, J. Review article: Understanding the pharmacodynamic and pharmacokinetic differences between proton pump inhibitors – focus on pKa and metabolism. *Aliment. Pharmacol. Ther. Symp. Ser.* **2006**, *2*, 340–350. [CrossRef]
29. Newton, D.W. Drug incompatibility chemistry. *Am. J. Health-Syst. Pharm.* **2009**, *66*, 348–357. [CrossRef] [PubMed]
30. Avdeef, A. *Absorption and Drug Development: Solubility, Permeability, and Change State*, 2nd ed.; Wiley: Hoboken, NJ, USA, 2012; pp. 22–24. [CrossRef]
31. Carbajo, J. Aplicación De La Fotocatálisis Solar a La Degradación De Contaminantes Orgánicos En Fase Acuosa Con Catalizadores Nanoestructurados De TiO_2. Ph.D. Thesis, Universidad Autónoma de Madrid, Madrid, España, 2013.
32. Yan, M.; Chen, F.; Zhang, J.; Anpo, M. Preparation of Controllable Crystalline Titania and Study on the Photocatalytic Properties. *J. Phys. Chem. B* **2005**, *109*, 8673–8678. [CrossRef] [PubMed]
33. Luttrell, T.; Halpegamage, S.; Tao, J.; Kramer, A.; Sutter, E.; Batzill, M. Why is anatase a better photocatalyst than rutile?—Model studies on epitaxial TiO_2 films. *Sci. Rep.* **2014**, *4*, 1–8. [CrossRef] [PubMed]
34. Sangchaya, W.; Sikonga, L.; Kooptarnonda, K. Comparison of photocatalytic reaction of commercial P25 and synthetic TiO_2-AgCl nanoparticles. *Procedia Eng.* **2012**, *32*, 590–596. [CrossRef]

35. Santiago, D.E.; Doña-Rodríguez, J.M.; Araña, J.; Fernández-Rodríguez, C.; González-Díaz, O.; Pérez-Peña, J.; Silva, A.M.T. Optimization of the degradation of imazalil by photocatalysis: Comparison between commercial and lab-made photocatalysts. *Appl. Catal. B-Environ.* **2013**, *138*, 391–400. [CrossRef]
36. Bianchi, C.L.; Gatto, S.; Pirola, C.; Naldoni, A.; Di Michele, A.; Cerrato, G.; Crocellà, V.; Capucci, V. Photocatalytic degradation of acetone, acetaldehyde and toluene in gas-phase: Comparison between nano and micro-sized TiO_2. *Appl. Catal. B-Environ.* **2014**, *146*, 123–130. [CrossRef]
37. Hossein, M.; Vosooghian, H. Photocatalytic degradation of some organic sulfides as environmental pollutants using titanium dioxide suspension. *J. Photochem. Photobiol. A Chem.* **2005**, *174*, 45–52. [CrossRef]
38. Stintzing, A. Solar Photocatalytic Treatment of Textile Wastewater at a Pilot Plant in Menzel Temime/Tunisia. Bachelor's Thesis, Institut für Thermische Verfahrenstechnik der Technischen Universität Clausthal, Clausthal, Germany, 2003.
39. Hemmens, V.J.; Moore, D.E. Photo-oxidation of 6-Mercaptopurine in Aqueous Solution. *J. Chem. Soc. Perkin Trans.* **1984**, *2*, 209–211. [CrossRef]
40. Kuhn, H.; Försterling, H. Kinetics of Chemical Reactions. In *Principles of Physical Chemistry*; Wiley: West Sussex, UK, 2000; pp. 677–682.
41. Lente, G. Facts and alternative facts in chemical kinetics: Remarks about the kinetic use of activities, termolecular processes, and linearization techniques. *Curr. Opin. Chem. Eng.* **2018**, *21*, 76–83. [CrossRef]